Showcasing research from Ming Li, School of Engineering, Macquarie University, Sydney, Australia, and Yaxiaer Yalikun, Division of Materials Science, Nara Institute of Science and Technology (NAIST), Nara, Japan.

Shape-based separation of drug-treated *Escherichia coli* using viscoelastic microfluidics

Cell shape is critical for modulating biological functions of Escherichia coli, a model bacterium with a number of roles in nature. The ability to prepare homogeneous E. coli populations adopting uniform shape or sort bacterial sub-populations based on their shape has significant implications for a broad range of biological, biomedical and environmental applications. Here, the authors achieved shape-based separation of antibiotic-treated E. coli by viscoelastic microfluidics.

As featured in:

ROYAL SOCIETY OF CHEMISTRY

rsc.li/loc

PAPER

Check for updates

Shape-based separation of drug-treated *Escherichia coli* using viscoelastic microfluidics†

Tianlong Zhang, [iD] [ab] Hangrui Liu, [iD] [a] Kazunori Okano, [b] Tao Tang, [iD] [b] Kazuki Inoue, [b] Yoichi Yamazaki, [b] Hironari Kamikubo, [b] Amy K. Cain, [iD] [c] Yo Tanaka, [iD] [d] David W. Inglis, [iD] [a] Yoichiroh Hosokawa, [b] Yalikun Yaxiaer*[b] and Ming Li [iD] *[ae]

Here, we achieve shape-based separation of drug-treated *Escherichia coli* (*E. coli*) by viscoelastic microfluidics. Since shape is critical for modulating biological functions of *E. coli*, the ability to prepare homogeneous *E. coli* populations adopting uniform shape or sort bacterial sub-population based on their shape has significant implications for a broad range of biological, biomedical and environmental applications. A proportion of *E. coli* treated with 1 μg mL⁻¹ of the antibiotic mecillinam were found to exhibit changes in shape from rod to sphere, and the heterogeneous *E. coli* populations after drug treatment with various aspect ratios (ARs) ranging from 1.0 to 5.5 were used for experiment. We demonstrate that *E. coli* with a lower AR, *i.e.*, spherical *E. coli* (AR ≤ 1.5), are directed toward the middle outlet, while rod-shaped *E. coli* with a higher AR (AR > 1.5) are driven to the side outlets. Further, we demonstrate that the separation performance of the viscoelastic microfluidic device is influenced by two main factors: sheath-to-sample flow rate ratio and the concentration of poly-ethylene-oxide (PEO). To the best of our knowledge, this is the first report on shape-based separation of a single species of cells smaller than 4 μm by microfluidics.

1. Introduction

Escherichia coli is a Gram-negative, rod-shaped model bacterium with a number of roles in nature ranging from commensal to pathogenic strains on human or animal hosts.[1] Typically, *E. coli* colonizes the human gastrointestinal tract and coexists in a mutually beneficial manner, playing an important role in the breakdown of particular carbon compounds.[2] However, pathogenic forms of *E. coli*, such as verotoxigenic (VTEC), enteroinvasive (EIEC) and uropathogenic/extraintestinal pathogenic (UPEC/ExPEC) classes, can undermine their hosts.[3] For example, *E. coli* O157:H7, a type of VTEC, has already caused mortality worldwide due to its resistance to low pH (~2.5), low infective dose (as few as 10 cells) and high pathogenicity.[4] Furthermore, *E. coli* can be regarded as an indicator of water quality.[5,6] *E. coli* is also a common model organism used in the laboratory for cloning, expression and mutagenesis studies to understand bacterial gene function and cellular processes.[7]

Shape is critical for modulating *E. coli* functions, such as attachment, motility, dispersal, predation and differentiation.[8–10] For example, an optimal aspect ratio (AR) of a rod-shaped *E. coli* cell allows it to move efficiently through liquids.[11] During the progress of forming intracellular communities, uropathogenic *E. coli* undergoes a rod–sphere–rod shape changes to fit the surrounding microenvironment.[12] Furthermore, studies have shown that the shape of *E. coli* can vary in response to external stimuli, such as antibiotic treatment,[9] temperature increase[13] and recurrent infections.[14] Given that *E. coli* is an important species in the fields of biotechnology and microbiology, and the most widely studied prokaryotic model organism, it is important to be able to separate *E. coli* populations based on their shape for the investigation of biological functions that result in cell shape change. Also, this precise morphologically-based sorting ability opens up avenues for various downstream applications,

ᵃ School of Engineering, Macquarie University, Sydney 2122, NSW, Australia. E-mail: ming.li@mq.edu.au
ᵇ Division of Materials Science, Graduate School of Science and Technology, Nara Institute of Science and Technology, 630-0192, Ikoma, Japan. E-mail: yaxiaer@ms.naist.jp
ᶜ ARC Centre of Excellence in Synthetic Biology, School of Natural Sciences, Macquarie University, Sydney 2122, NSW, Australia
ᵈ Center for Biosystems Dynamics Research, RIKEN, Osaka 565-0871, Japan
ᵉ Biomolecular Discovery Research Centre, Macquarie University, Sydney 2122, NSW, Australia
† Electronic supplementary information (ESI) available. See DOI: https://doi.org/10.1039/d2lc00339b

including biochemical assays, mutational analysis and next generation sequencing.

Unfortunately, there has been very little research reported on shape-based separation of cells using traditional separation approaches, such as filtration, centrifuge and fluorescence-activated cell sorting (FACS), as shape has not often been considered in these approaches. Microfluidics, a technology characterized by the engineered manipulation of fluids at the sub-millimeter scale,[15] has attracted growing interest for the manipulation and separation of particles (both synthetic and biological) due to its desirable features, including miniaturization, precise control of fluids, rapid sample processing, low reagent consumption and fast analysis.[16–20] By now, microfluidic technology has enabled a broad range of applications, such as particle rotation,[21] focusing,[22,23] mixing,[24] detection,[25] separation[26] and droplet generation.[27] Several microfluidic separation techniques have been reported for shape-based separation of particles, which can be classified into two groups: active approaches based on external actuation fields, and passive approaches depending on channel geometry or medium properties.[28,29] For example, electrical and magnetic forces have been used for the separation of spherical (5 μm in diameter) and peanut-shaped (3.5 μm in width and 6 μm in length) polystyrene particles of similar volume,[30] and the separation of spherical (7 μm in diameter) and prolate ellipsoidal magnetic particles of the same volume,[31] respectively. However, these active approaches always require extra device fabrication or bulky external setup.

Moreover, passive methods like inertial focusing,[32] deterministic lateral displacement (DLD)[33] and viscoelastic microfluidics[34] have been used for shape-based particle separation. For example, inertial focusing has been reported for separating spherical (6 μm in diameter) and ellipsoidal polystyrene particles of the same volume[32] and microalga *Euglena gracilis* populations with different ARs.[35] DLD technique has enabled shape-based separation of three types of red blood cells (*i.e.*, discocytes, echinocytes and stomatocytes),[34] and separation of spherical and non-spherical bacterial populations.[36] However, inertial microfluidics is limited to relatively larger particles (*i.e.*, >6 μm)[32] and DLD suffers from complicated fabrication process. In recent years, viscoelastic microfluidics has been widely adopted for shape-based separation of different types of microbial cells, such as *Candida Albicans* (≥26 μm),[37] *Saccharomyces Cerevisiae* (singlets: ∼3 to 5 μm, doubles and clusters),[38] *Cyanobacterial Anabaena* (∼5 μm in diameter and a few microns to hundreds of microns in length)[34] and *Bacillus subtilis* (*i.e.*, 1–5 um and >20 μm in length).[39] However, it has not been shown whether viscoelastic microfluidics can be used to separate a single species of bacteria with relatively small size (∼0.5 to 4 μm) based on cell shape.

In this study, we achieve shape-based separation of antibiotic-treated *E. coli* with a major axis mainly ranging from 0.5 to 4 μm using viscoelastic microfluidics. The shape-based separation is further proven by analysing AR values of volume equivalent *E. coli* populations at different outlets. To the best of our knowledge, it is the first report on shape-based separation of a single species of cells smaller than 4 μm by microfluidics. Sub-populations of *E. coli* cultures treated with the beta-lactam antibiotic mecillinam exhibit change in shape from rod to sphere (AR ≤ 1.5), likely because they become cell-wall deficient l-forms variants.[14] We use a co-flow of viscoelastic (sheath) and Newtonian fluids (sample) to separate *E. coli* with different ARs ranging from 1.0 to 5.5 by shape in a straight microchannel. Under the combined effects of the net inertial lift and elastic forces, sphere-shaped *E. coli* (AR ≤ 1.5) exit from the middle outlet while rod-shaped *E. coli* (AR > 1.5) are more likely to exit from side outlets. Also, the influence of different factors, such as injection total flow rate, sheath-to-sample flow rate ratio and poly-ethylene-oxide (PEO) concentration, on the separation performance of the viscoelastic microfluidic device were studied. Given the biological, biomedical and environmental importance of *E. coli*, this device is expected to be adopted by wider scientific communities in various fields of microbiology, biotechnology and cell biology for various biological applications.

2. Theory

Particle migration in a straight microchannel by viscoelastic microfluidics is governed by the combined effects of the net inertial lift force F_L (comprised of shear gradient lift F_{L_S} and wall lift F_{L_W}) and elastic force (F_E).[40] F_{L_S} pushes a neutrally buoyant particle toward the adjacent channel wall while the wall lift pushes the particle away from the wall to the channel center.[38] Here, $F_L = F_{L\_S} + F_{L\_W} = \rho_f V_m d^4 D_h^{-2} f_L$, where ρ_f is fluid density, V_m is mean flow velocity, d, D_h and f_L are particle diameter, channel hydraulic diameter and inertial lift coefficient, respectively. However, F_L becomes insignificant for particles smaller than a few microns, since it drops dramatically with the decrease in particle diameter.

Reorientation and alignment of macromolecules along the flow direction accompany normal stresses in viscoelastic fluids. The elastic force (F_E) arising from the first normal stress (N_1) difference drives particles toward centreline where shear rate is the lowest. $F_E = C_{el} d^3 \nabla N_1$ (where C_{el} is elastic lift coefficient)[40] is significant for particles smaller than a few microns.[22] Here, the first normal stress N_1 is defined as the difference between the streamwise normal stress (σ_{xx}) and the transverse normal stress (σ_{yy}), where the coordinate system is set such that x is in the downstream flow direction and y is in the direction perpendicular to the x direction.[41] Therefore, changes in the factors, such as concentration of viscoelastic medium, particle size, channel dimensions and fluid velocity, can influence the behavior of the cross-stream migration of the particle.

In viscoelastic fluids, Reynolds number (Re) and Weissenberg number (Wi) can be used for the characterization of inertial and viscoelastic effects.[41]

Elasticity number (El) is used for evaluating the relative importance of the elastic and inertial forces. $Re = \rho V_m D_h / \eta$, where η is the fluid dynamic viscosity. $Wi = \lambda \dot{\gamma}$, where λ is relaxation time and $\dot{\gamma}$ is the shear rate. $El = Wi/Re$. Table S1 and S2† showed the values of the three dimensionless parameters used in this study.

3. Materials and methods

3.1 Device fabrication

The SU-8 mold (SU-83050, Tokyo Ohka Kogyo, Tokyo, Japan) was fabricated on a silicon wafer using standard photolithography. The poly(dimethylsiloxane) (PDMS, Sylgard 184, Dow Corning, Midland, MI, USA) mixture was prepared by mixing the base and the curing agent with a weight ratio of 10 : 1. After mixing, degassing was conducted under vacuum for 30 min. Then the PDMS mixture was poured over the mold and baked in an oven at 80 °C for 3 h. After peeling the PDMS layer off the mold, the holes for the inlets and outlets were punched. Then, the PDMS microchannel was bonded to the glass substrate (Neo Micro Cover Glass, 60 × 24 × 0.13–0.17 mm, Matsunami Glass Ind., Ltd.) through 40-second plasma treatment (Plasma Cleaner CY-P2L-B). The glass slide was cleaned with 70% alcohol and then dried by nitrogen blast before the plasma treatment.

3.2 PEO medium preparation

PEO powder (molecular weight M_w of 600 kDa, 182 028, Sigma-Aldrich, St. Louis, MO) was dissolved using phosphate buffered saline (PBS) in a 50 mL plastic centrifuge tube (Kartell) to get PEO solutions with two concentrations: 200 and 1000 parts per million (ppm). To avoid PEO aggregates, the tube was shaken overnight at 23 °C by a triple shaker (NR-80, TAITEC Ltd., Japan) at 150 revolutions per minute (rpm) to accelerate the dissolution.

3.3 Cell preparation

E. coli, XL2-Blue (Stratagene), were cultured at 37 °C in lysogeny broth (LB) media and passaged every 12 to 16 hours. *E. coli* were treated with a subinhibitory concentration (1 µg mL⁻¹) of mecillinam, a specific inhibitor of penicillin-binding protein 2 (PBP2),[42,43] for 8 hours to induce shape change.[44] 70% alcohol was used for cell fixing at 23 °C. To avoid forming aggregates, the cell–alcohol mixtures were manually stirred and then placed in the triple shaker at 100 rpm for ~2 hours. After fixation, cells were centrifuged at 3000 rpm for 30 min, followed with the washing by PBS solution three times. Finally, the fixed cells were suspended with PBS solution and stored at 4 °C in a refrigerator. In the experiment, the fixed mecillinam-treated *E. coli* cells were used. Before injecting into the microchannel, *E. coli* solution was mixed with 0.1% Tween 20 solution at the ratio of 1 : 1, shaken with a mixer (Automatic Lab-Mixer HM-lOH, Iuchi) for 30 seconds, and filtered by a 20 µm non-sterile filter (PluriStrainer, PluriSelect).

3.4 Experimental setup

E. coli sample and PEO sheath solutions were injected into the microchannel using two syringe pumps (Harvard Apparatus 11 Elite) *via* two 1 mL Terumo syringes. The microfluidic device was placed under an inverted microscope (Zeiss Axiovert 100 microscope) equipped with a high-speed camera (Keyence VW-600C, America). Differential interference contrast (DIC) and a 100× oil immersion objective lens (Olympus; Plan N, NA = 1.30) were used for observation. A schematic of the observation system was shown in ESI† Fig. S1. The software Motion Analyzer VW 9000 (Keyence, Osaka, Japan) was used to record the trajectories of *E. coli* at 4000 to 6000 frames per second (fps). Minor and major axis of *E. coli* were measured using software ImageJ. Cell aspect ratio (AR = major axis/minor axis) and volume were calculated.

3.5 Separation performance evaluation

We used three levels of AR to evaluate the distributions for *E. coli* having different shapes at the inlet and outlets. Here, AR = 1, AR = 2 and AR ≥ 3 mean that AR ranges from 1.0 to 1.5, 1.5 to 2.5 and >2.5, respectively. Also, extraction purity (EP) and enrichment factor (EF) were used to evaluate the separation efficiency.[35,38] EP represents the proportion of *E. coli* with a specific AR at the inlet and each outlet; EF is defined as the proportion of *E. coli* with a specific AR (*e.g.*, AR = 1) at a given outlet to the proportion of *E. coli* with the same AR (*e.g.*, AR = 1) at the inlet.

4. Results and discussion

4.1 Device design

The viscoelastic microfluidic device for shape-based *E. coli* separation consists of two inlets for the injection of sheath and sample solutions, a straight rectangular microchannel (15 mm long and 20 µm wide) and seven outlets (Fig. 1A). The PDMS microchannel is 50 µm in height. O1, O2, O2′, O3, O3′, O4 and O4′ denote seven outlets. Here, the blockage ratio ($\beta = d/D_h$) is much lower than 0.25, ensuring that larger sphere-shaped *E. coli* can be driven toward the channel centre.[40,45] A serpentine resistance microchannel (see ESI† Fig. S2) was designed before each outlet to reduce the effects of reservoir fluid height and capillary pressure on the flow distribution.[39] The ratio of the serpentine channel length relative to the main focusing channel length is about 0.51. Since the seven channel outlets are symmetric about the channel centreline (see Fig. 1A), we only collected and compared *E. coli* populations from four outlets (O1–O4). Representative experimental images of initial *E. coli* population at the inlet and collected *E. coli* subpopulations at the outlets were shown (Fig. 1B). Under the combined effects of elastic and inertial lift forces, *E. coli* with lower ARs were driven to the middle outlet O1 while *E. coli* with relatively higher ARs mainly exit from the side outlets (*e.g.*, O3 and O4), demonstrating shape-based separation of *E. coli* by viscoelastic microfluidics.
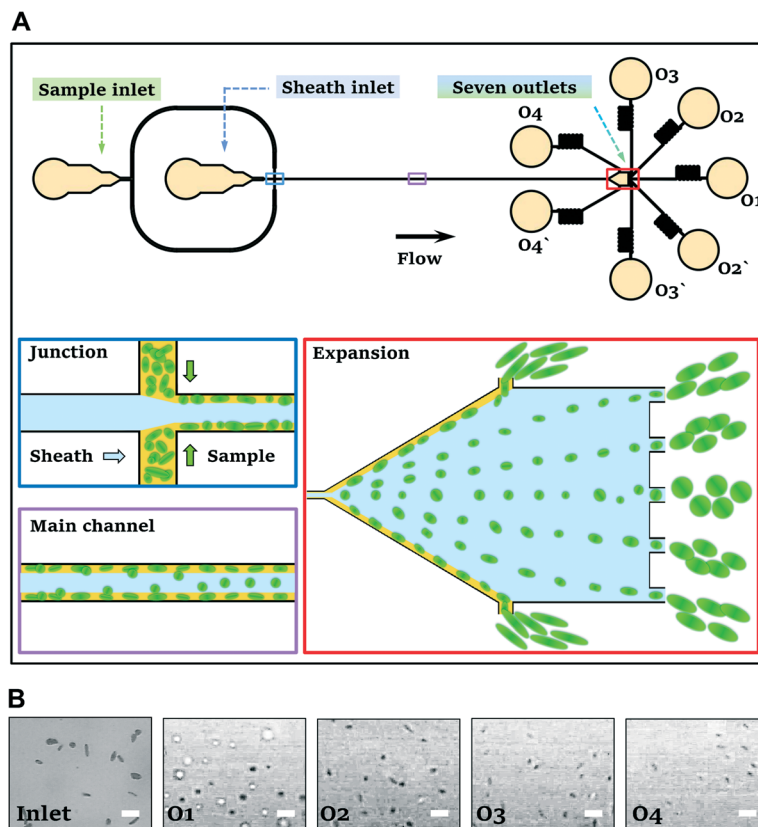
Fig. 1 The design of the viscoelastic microfluidic device for shape-based separation of drug-treated *E. coli*. (A) Schematics of the microfluidic device used for *E. coli* separation by shape. (B) Experimental images of initial *E. coli* population at the inlet and *E. coli* subpopulations at four outlets O1, O2, O3 and O4 after separation. Scale bar is 5 μm.

We found that mecillinam treatment caused 33.7% of *E. coli* to take sphere-like shapes after fixing ($N = 300$). We compared the rod-shaped *E. coli* in the untreated control group (Fig. 2A) to the drug-treated group (Fig. 2B). After mecillinam treatment, both the major and minor axis of *E. coli* cells increased (Fig. 2C) and a decrease in the AR of *E. coli* was detected (Fig. 2D). Mecillinam-treated *E. coli* exhibit various ARs ranging from 1.0 to 5.5,

and the average AR values in the treatment group and control group were 1.98 ± 0.79 and 2.94 ± 1.04, respectively.

4.2 Shape-based separation of *E. coli*

We examined the separation of *E. coli* with ARs ranging from 1.0 to 5.5 at the outlets, where sheath and sample solutions
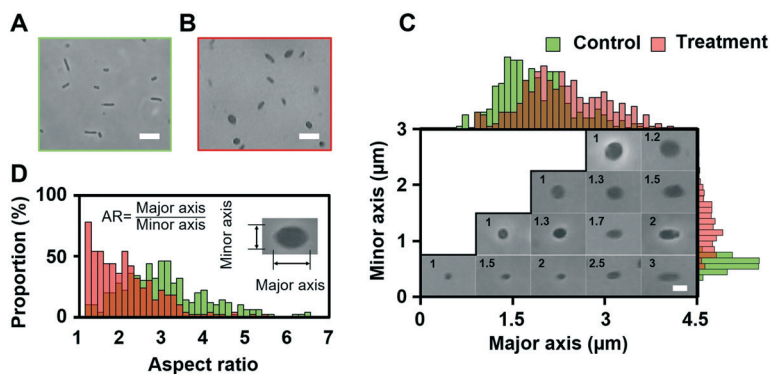

Fig. 2 The change in the shape of *E. coli* due to mecillinam treatment. (A and B) Images of *E. coli* without (A) and with mecillinam treatment (B) after fixation. Scale bar is 5 μm. (C) Distributions of the major and minor axis of *E. coli* with and without drug treatment. The numbers within the images denote AR values. Scale bar is 2 μm. (D) Distributions of AR of *E. coli* in control and mecillinam-treated groups. $N = 300$.
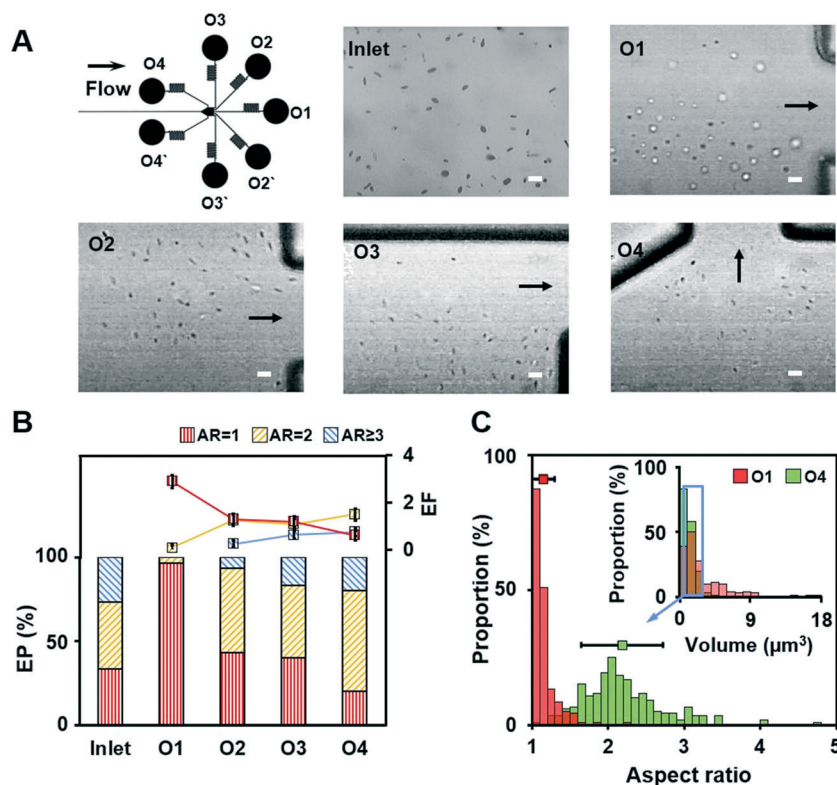
Fig. 3 Shape-based separation of drug-treated *E. coli* by viscoelastic microfluidics. The flow rates of sheath and sample solutions are 8 and 2 μL min^{-1}, respectively, and PEO concentration is 1000 ppm. (A) Representative experimental images of *E. coli* at the inlet and four outlets: O1, O2, O3 and O4. Black arrows denote the flow direction. Scale bar is 5 μm. (B) Plots of extraction purity (EP) and enrichment factor (EF) for three groups of *E. coli* with different ARs for each outlet. N = 30 for each group. (C) Comparison of aspect ratio of *E. coli* collected from outlets O1 and O4. The blue rectangle denotes selected *E. coli* with the same volume at the two outlets for aspect ratio analysis. N = 300.

were injected at 8 and 2 μL min^{-1}, respectively, when PEO concentration was 1000 ppm. The corresponding Re was 4.1 and Wi was 9.3. Sphere-shaped *E. coli* were found to be directed to outlet O1 while rod-shaped *E. coli* mainly exited from outlet O4 (Fig. 3A). Videos demonstrating the flowing of the sphere-shaped and rod-shaped *E. coli* toward O1 and O4, respectively, are provided (see Video S1 and S2†). The EP of sphere-shaped *E. coli* (AR = 1) at O1 exhibited a decreasing tendency from O1 (96.7%) to O4 (20.0%) (Fig. 3B). Similarly, the EF of sphere-shaped *E. coli* (AR = 1) decreased from 2.9 (at O1) to 0.6 (at O4). Moreover, *E. coli* exit from outlet O1 and O4 were collected and analysed (Fig. S3†). We compared the major and minor axis of *E. coli* collected from O1 and O4, and calculated cell volume using equation $V = \pi a b^2/6$ (where a and b refer to the major and minor axis of *E. coli*, respectively; Fig. 3C insert). We noted that sphere-like *E. coli* smaller than 1 μm were driven to outlet O1 (see Fig. S3A†), demonstrating that this viscoelastic microfluidic device can be used for cell separation at the nanoscale.

We supposed that *E. coli* are subjected to both a size-dependent force and a shape-dependent force when flowing through the microchannel. To demonstrate that the separation is mainly dependent on shape rather than size, we selected *E. coli* with the same volume from O1 and O4 (highlighted by blue rectangle in Fig. 3C insert and Fig. S3B†)

by removing outliner cells. By analysing *E. coli* populations with the same volume, we eliminated the effects of cell size on the separation. Then we compared AR of *E. coli* with the same volume at O1 and O4. The results showed that the average AR values of *E. coli* populations with the same volume at O1 and O4 are 1.14 ± 0.15 and 2.18 ± 0.53, respectively (Fig. 3C), proving shape-based separation at the outlets. Therefore, we conclude that the separation of *E. coli* is mainly shape-dependent rather than size-dependent.

4.3 Separation affected by sheath-to-sample ratio and total flow rate

To study the influence of the flow rate ratio (FRR) of sheath to sample on the separation, we maintained a constant total flow rate (Q_t) of 10 μL min^{-1}, but adjusted the sheath (Q_{sh}) and sample flow rate (Q_s) to render two different FRRs (FRR = Q_{sh}/Q_s): 1.5 (Q_{sh} = 6 μL min^{-1}, Q_s = 4 μL min^{-1}) and 9 (Q_{sh} = 9 μL min^{-1}, Q_s = 1 μL min^{-1}). The PEO concentration was fixed at 1000 ppm. The Re and Wi values were 4.1 and 9.3, respectively (see Table S2†). Representative experimental images at O2 were shown (Fig. 4A).

In all conditions, we found out that sphere-shaped and rod-shaped *E. coli* were mainly exit from middle outlet (O1) and side outlet (O4), respectively (Fig. 4B). In the FRR = 1.5
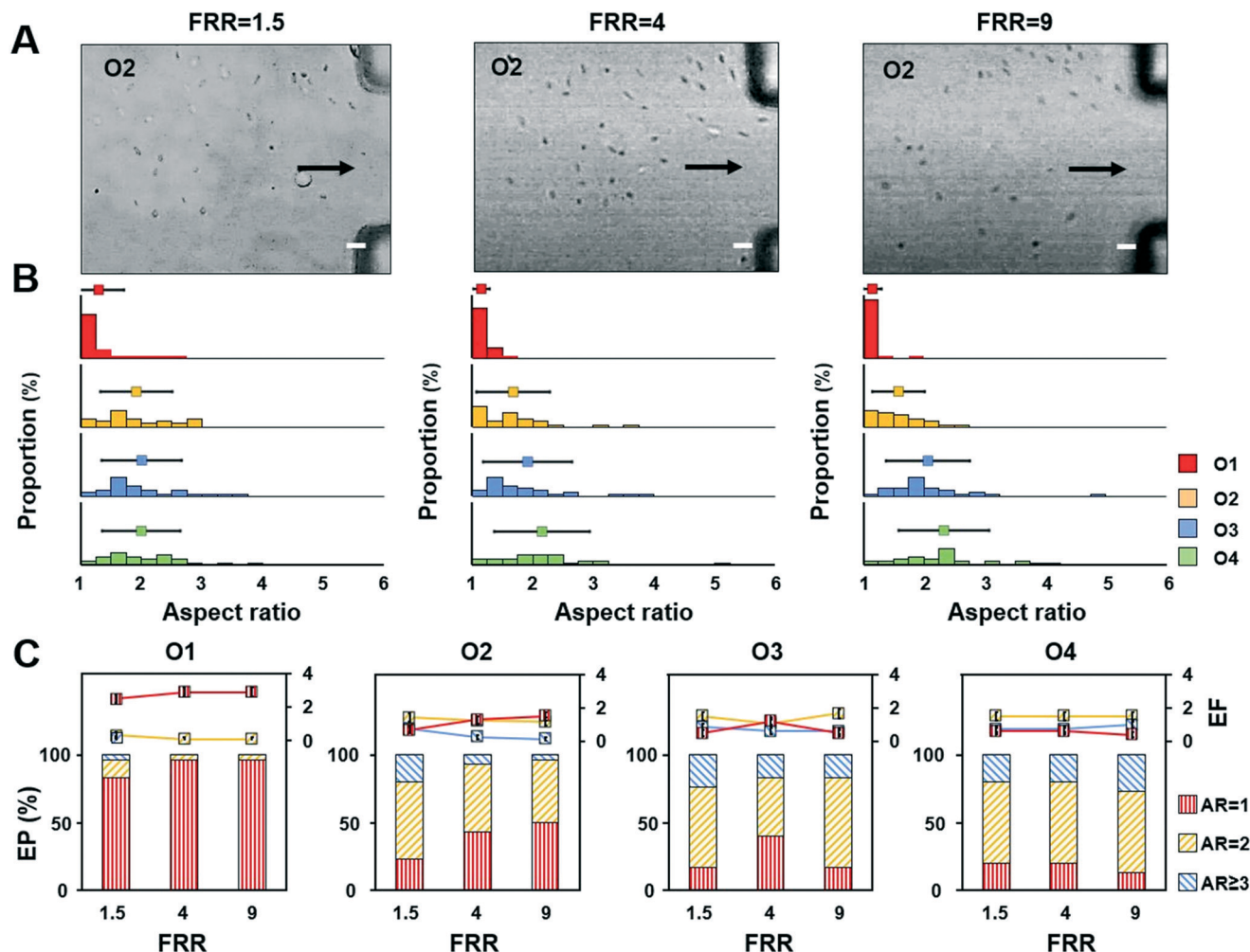
Fig. 4 Shape-based separation of *E. coli* by viscoelastic microfluidics under the effects of sheath-to-sample flow rate ratio (FRR). The total flow rate is fixed at 10 μL min^{-1} and PEO concentration is 1000 ppm. (A) Experimental images *E. coli* at the outlet O2 at three different FRRs: (left) 1.5, (middle) 4 and (right) 9. Black arrows denote the flow direction. Scale bar is 5 μm. (B) Distributions of aspect ratio of *E. coli* at four outlets at three different FRRs: (left) 1.5, (middle) 4 and (right) 9. (C) Enrichment factor (EF) and extraction purity (EP) in different FRR conditions at four outlets O1, O2, O3 and O4. *N* = 30.

condition, the average AR value in O1 was 1.29 ± 0.42, which was slightly higher than the ones in FRR = 4 (1.15 ± 0.14) and in FRR = 9 condition (1.15 ± 0.15). Similar to FRR = 4 condition, we also found nanoscale spherical *E. coli* at O1 in FRR = 9 (Fig. S4†). When FRR was increased from 1.5 to 9, the average AR value of *E. coli* at O2 decreased from 1.91 ± 0.60 to 1.59 ± 0.44, indicating that more spherical *E. coli* were driven toward channel centre at higher FRR conditions. The average AR values at O3 and O4 were higher in FRR = 9 condition than the ones in FRR = 4 and FRR = 1.5 conditions, indicating that more rod-shaped *E. coli* are driven toward channel sidewall in FRR = 9 condition. We further analysed and compared EF and EP at four outlets O1, O2, O3 and O4 (Fig. 4C). EF and EP values of sphere-shaped *E. coli* with AR = 1 at O1 are relatively higher in the FRR = 9 (EF = 2.9, EP = 96.7%) and FRR = 4 conditions (EF = 2.9, EP = 96.7%) than the ones in FRR = 1.5 condition. When increasing FRR from 1.5 to 9, EP (23.3% to 50.0%) and EF (0.7 to 1.5) values of

sphere-shaped *E. coli* (AR = 1) at middle outlet (O2) demonstrated an increasing tendency, suggesting that sphere-shaped *E. coli* cells are more likely to be driven toward channel centre at a higher FRR.

Taken together, higher FRR exhibited a stronger ability to drive sphere-shaped *E. coli* (AR = 1) to the channel center, resulting in different lateral positions under different flow conditions. Whilst, more rod-shaped *E. coli* were found to be driven to the channel center at a lower FRR condition, *e.g.*, FRR = 1.5. The relative importance of elastic and inertial lift force is the same for the three FRR conditions (El = 2.28). FRR can influence the proportion of sphere-shaped *E. coli* that directly interact with the sheath fluids. Particularly, a higher FRR (*e.g.*, FRR = 9) generated an interface between the sample and sheath flows closer to the sidewall of the microchannel, allowing a higher degree of opportunity of the interaction between sphere-shaped *E. coli* with sheath flow in the microchannel.
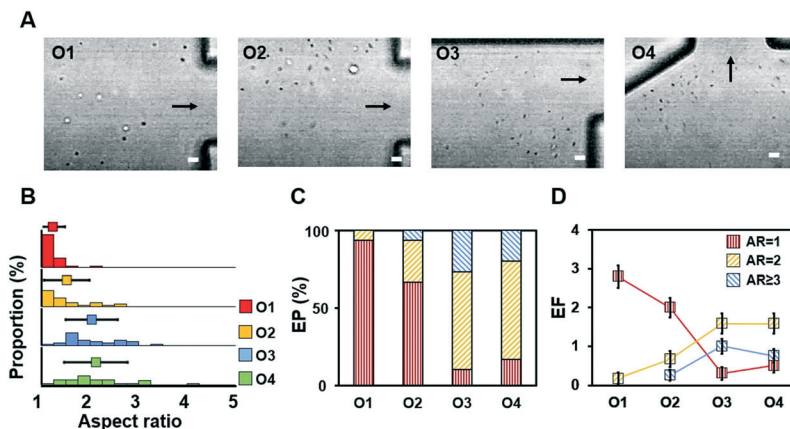
Fig. 5 Shape-based separation of *E. coli* by viscoelastic microfluidics when PEO concentration is 200 ppm. The sheath and sample flow rates are 8 and 2 μL min^{-1}, respectively. (A) Representative experimental images of *E. coli* flowing toward different outlets. Black arrows denote *E. coli* flow directions. Scale bar is 5 μm. (B) Distributions of aspect ratio of *E. coli* collected at different outlets. (C) Extraction purity (EP) and (D) enrichment factor (EF) of three groups of *E. coli* with different ARs at four outlets: O1, O2, O3 and O4. N = 30 for each group.

Moreover, the effect of total flow rates (TFR) on the separation performance of the viscoelastic microfluidic device was investigated (see ESI† Fig. S5). The FRR was constant at 4, while TFR was adjusted to either 5 μL min^{-1} (Q_{sh} = 4 μL min^{-1}, Q_s = 1 μL min^{-1}) or 20 μL min^{-1} (Q_{sh} = 16 μL min^{-1}, Q_s = 4 μL min^{-1}). The PEO concentration was 1000 ppm. Representative experimental images at O2 were shown (Fig. S5A†). The difference in the average AR value of *E. coli* at O1 between TFR = 10 (1.15 ± 0.14), TFR = 5 (1.21 ± 0.28) and TFR = 20 (1.21 ± 0.26) was not significant (Fig. S5B†). Sphere-shaped *E. coli* (AR = 1) at O1 showed slightly higher values of EF and EP (EP = 96.7%, EF = 2.9) in TFR = 10 condition than the other two conditions (TFR = 5 and 20, Fig. S5C†). We find that the separation performance is relatively stable when TFR increases from 5 to 20. The mechanism relationship between the TFR-dependent results is interesting yet warrants future investigation.

4.4 Separation affected by PEO concentration

To explore the influence of PEO concentration on the separation performance of the viscoelastic microfluidic device, we further prepared sheath solutions containing PEO at a concentration of 200 ppm. The sheath and sample solutions were injected at 8 and 2 μL min^{-1}, respectively (TFR = 10 μL min^{-1}, FRR = 4). The Re value is 5.32, the Wi value is 3.28 and El is 0.62 (see Table S1†).

We observed and compared the distributions of *E. coli* varying in AR at the four outlets (Fig. 5A). The results showed that AR values of *E. coli* at the outlets increased with the increase of the distance from channel centre to channel sidewall: O1 (1.21 ± 0.25) *vs.* O4 (2.10 ± 0.66). This indicated that there were less sphere-shaped but more rod-shaped *E. coli* at the outlet closer to channel sidewall (Fig. 5B). This was further reflected by analysing EP and EF for three groups of *E. coli* with different ARs at the outlets. Sphere-shaped *E. coli* (AR = 1) at O1 have

a relatively higher EP and EF of 93.3% and 2.8, respectively, than those collected at the other outlets (Fig. 5C and D).

Compared with the 1000 ppm condition (El = 2.28), the 200 ppm condition (El = 0.61) resulted in a decrease in the relative importance of elastic and inertial lift forces, which means the elastic force that drives the sphere-shaped *E. coli* toward the channel center is smaller. This is evidenced by a higher EP and EF for sphere-shaped *E. coli* (AR = 1) at O2 in the 200 ppm condition (EP = 66.7%, EF = 2) than the 1000 ppm condition (EP = 43.3%, EF = 1.3). To improve the throughput, we will consider improving cell concentration, optimising the width and depth of the main microchannel and using multiple microchannels arranged in a cascade way[46] in the future research.

5. Conclusion

In our work, sphere-shaped *E. coli* (AR ≤ 1.5) were able to be directed to the center of the microchannel. However, a portion of rod-shaped *E. coli* with equal volume were not center directed, resulting in their exit from outlets closer to channel sidewalls. We noted that a similar design was used for size-based separation of spherical polystyrene particles, *e.g.*, 1 and 2 μm,[47] and 0.1 and 0.5 μm,[48] using viscoelastic microfluidics. In these two studies, larger spherical particles, *e.g.*, 2- and 0.5 μm ones, were able to be directed toward the channel center by adjusting flow rates and PEO concentration. Despite that several studies have investigated the fluidic dynamics of the rod-shaped or ellipsoidal particles,[32,49–52] we failed to find any studies that can explain the physics of rod-shaped *E. coli* flowing in the streams closer to the channel sidewalls in this study. Since the rod-shaped *E. coli* is not spherically symmetric in shape, there is a lack of stable elastic force exerted on the cells to drive them laterally toward the channel center. Also, the rod-shaped *E. coli* may experience less rotation which may result in less

rotation-induced wall lift force, leading to less capability in migration toward channel center.[53]

In this work, we demonstrated the first shape-based separation of antibiotic-treated *E. coli* by viscoelastic microfluidics in a label-free and continuous manner. *E. coli* cells with various ARs ranging from 1.0 to 5.5 were found to mainly exit from different outlets. Sphere-shaped *E. coli* (AR ≤ 1.5) were found to have a high EP of 96.7% at the outlet in the channel center (O1), while rod-shaped *E. coli* (AR > 1.5) were mainly collected from the outlet closest to the channel sidewall (O4). The performance of the viscoelastic microfluidic device for shape-based *E. coli* separation was found to be affected by sheath-to-sample ratio and PEO concentration. Future work can build upon this proof-of-concept study to further optimise conditions for shape-based separation of *E. coli* in terms of flow rates, PEO concentration and microchannel geometry *etc.* This technology will allow downstream genomics experiments on the separated *E. coli* populations to determine linkage between cell shape, antibiotic susceptibility and gene function. The developed microfluidic platform is expected to be adopted by broad scientific communities for different applications in the fields of microbiology, molecular biology and biomedicine.

Author contributions

M. Li, Y. Yalikun and T. Zhang conceived the idea. T. Zhang, Y. Yalikun, Y. Hosokawa and M. Li designed the work. T. Zhang, Y. Yamazaki, H. Kamikubo and Y. Yalikun prepared bacteria samples. T. Zhang, K. Okano, T. Tang, K. Inoue, Y. Tanaka and Y. Yalikun conducted the experiments. T. Zhang, AK Cain, D. Inglis and M. Li performed data analysis. Y. Yalikun and M. Li supervised the work. T. Zhang, H. Liu, AK Cain, D. Inglis, Y. Hosokawa, Y. Yalikun and M. Li wrote the manuscript.

Conflicts of interest

The authors declare no competing interests.

Acknowledgements

References

1 X. Chen, L. Zhou, K. Tian, A. Kumar, S. Singh, B. Prior and Z. Wang, *Biotechnol. Adv.*, 2013, **31**, 1200–1223.

2 J. B. Kaper, J. P. Nataro and H. L. T. Mobley, *Nat. Rev. Microbiol.*, 2004, **2**(2), 123–140.

3 J. van Elsas, A. Semenov, R. Costa and J. Trevors, *ISME J.*, 2011, **5**, 173–183.

4 J. Tilden, W. Young, A. McNamara, C. Custer, B. Boesel, M. Lambert-Fair, J. Majkowski, D. Vugia, S. Werner, J. Hollingsworth and J. Morris, *Am. J. Public Health*, 1996, **86**, 1142–1145.

5 S. Edberg, E. Rice, R. Karlin and M. Allen, *J. Appl. Microbiol.*, 2000, **88**, 106S–116S.

6 S. T. Odonkor and J. K. Ampofo, *Microbiol. Res.*, 2013, **4**, 5–11.

7 I. M. Keseler, S. Gama-Castro, A. Mackie, R. Billington, C. Bonavides-Martínez, R. Caspi, A. Kothari, M. Krummenacker, P. E. Midford, L. Muñiz-Rascado, W. K. Ong, S. Paley, A. Santos-Zavaleta, P. Subhraveti, V. H. Tierrafría, A. J. Wolfe, J. Collado-Vides, I. T. Paulsen and P. D. Karp, *Front. Microbiol.*, 2021, **12**, 711077.

8 K. Young, *Microbiol. Mol. Biol. Rev.*, 2006, **70**, 660–703.

9 K. Huang, R. Mukhopadhyay, B. Wen, Z. Gitai and N. Wingreen, *Proc. Natl. Acad. Sci. U. S. A.*, 2008, **105**, 19282–19287.

10 K. D. Young, *Curr. Opin. Microbiol.*, 2007, **10**, 596–600.

11 S. Cooper and M. W. Denny, *FEMS Microbiol. Lett.*, 1997, **148**, 227–231.

12 S. S. Justice, C. Hung, J. A. Theriot, D. A. Fletcher, G. G. Anderson, M. J. Footer and S. J. Hultgren, *Proc. Natl. Acad. Sci. U. S. A.*, 2004, **101**, 1333–1338.

13 K. J. Begg and W. D. Donachie, *J. Bacteriol.*, 1985, **163**, 615–622.

14 K. M. Mickiewicz, Y. Kawai, L. Drage, M. C. Gomes, F. Davison, R. Pickard, J. Hall, S. Mostowy, P. D. Aldridge and J. Errington, *Nat. Commun.*, 2019, **10**, 1–9.

15 E. K. Sackmann, A. L. Fulton and D. J. Beebe, *Nature*, 2014, **507**, 181–189.

16 G. M. Whitesides, *Nature*, 2006, **442**, 368–373.

17 D. B. Weibel and G. M. Whitesides, *Curr. Opin. Chem. Biol.*, 2006, **10**, 584–591.

18 T. Tang, Y. Yuan, Y. Yalikun, Y. Hosokawa, M. Li and Y. Tanaka, *Sens. Actuators, B*, 2021, **339**, 129859.

19 T. Zhang, Y. Shen, R. Kiya, D. Anggraini, T. Tang, H. Uno, K. Okano, Y. Tanaka, Y. Hosokawa, M. Li and Y. Yalikun, *Biosensors*, 2021, **11**, 263.

20 D. Anggraini, N. Ota, Y. Shen, T. Yo, Y. Hosokawa, M. Li and Y. Yalikun, in *In Handbook of Single-Cell Technologies*, Springer, 2021, pp. 287–310.

21 T. Tang, Y. Hosokawa, T. Hayakawa, Y. Tanaka, W. Li, M. Li and Y. Yalikun, *Engineering*, 2021, 1600205.

22 T. Zhang, Z. Y. Hong, S. Y. Tang, W. Li, D. W. Inglis, Y. Hosokawa, Y. Yalikun and M. Li, *Lab Chip*, 2020, **20**, 35–53.

23 T. Zhang, M. Namoto, K. Okano, E. Akita, N. Teranishi, T. Tang, D. Anggraini, Y. Hao, Y. Tanaka, D. Inglis, Y. Yalikun, M. Li and Y. Hosokawa, *Sci. Rep.*, 2021, **11**, 1–10.

24 S. Lee, D. van Noort, J. Lee, B. Zhang and T. Park, *Lab Chip*, 2009, **9**, 479–482.

25 D. Pekin, Y. Skhiri, J. Baret, D. le Corre, L. Mazutis, C. Salem, F. Millot, A. el Harrak, J. Hutchison, J. Larson, D.

Link, P. Laurent-Puig, A. Griffiths and V. Taly, *Lab Chip*, 2011, **11**, 2156–2166.

26 W. Zhang, K. Kai, D. Choi, T. Iwamoto, Y. Nguyen, H. Wong, M. Landis, N. Ueno, J. Chang and L. Qin, *Proc. Natl. Acad. Sci. U. S. A.*, 2012, **109**, 18707–18712.

27 H. Liu, X. Xu, K. Peng, Y. Zhang, L. Jiang, T. C. Williams, I. T. Paulsen, J. A. Piper and M. Li, *Biotechnol. Bioeng.*, 2021, **118**, 647–658.

28 C. Shields, C. Reyes and G. López, *Lab Chip*, 2015, **15**, 1230–1249.

29 Y. Shen, Y. Yalikun and Y. Tanaka, *Sens. Actuators, B*, 2019, **282**, 268–281.

30 J. DuBose, X. Lu, S. Patel, S. Qian, S. W. Joo and X. Xuan, *Biomicrofluidics*, 2014, **8**, 014101.

31 R. Zhou, F. Bai and C. Wang, *Lab Chip*, 2017, **17**, 401–406.

32 M. Masaeli, E. Sollier, H. Amini, W. Mao, K. Camacho, N. Doshi, S. Mitragotri, A. Alexeev and D. di Carlo, *Phys. Rev. X*, 2012, **2**, 031017.

33 J. McGrath, M. Jimenez and H. Bridle, *Lab Chip*, 2014, **14**, 4139–4158.

34 D. Yuan, S. Yan, J. Zhang, R. M. Guijt, Q. Zhao and W. Li, *Anal. Chem.*, 2021, **93**, 12648–12654.

35 M. Li, H. E. Muñoz, K. Goda and D. di Carlo, *Sci. Rep.*, 2017, **7**, 10802.

36 S. Ranjan, K. K. Zeming, R. Jureen, D. Fisher and Y. Zhang, *Lab Chip*, 2014, **14**, 4250–4262.

37 J. Nam, H. Jee, W. S. Jang, J. Yoon, B. G. Park, S. J. Lee and C. S. Lim, *Micromachines*, 2019, **10**, 817.

38 P. Liu, H. Liu, D. Yuan, D. Jang, S. Yan and M. Li, *Anal. Chem.*, 2021, **93**, 1586–1595.

39 P. Liu, H. Liu, L. Semenec, D. Yuan, S. Yan, A. K. Cain and M. Li, *Microsyst. Nanoeng.*, 2022, **8**, 1–11.

40 D. Yuan, Q. Zhao, S. Yan, S. Y. Tang, Y. Zhang, G. Yun, N. T. Nguyen, J. Zhang, M. Li and W. Li, *Lab Chip*, 2019, **19**, 2811–2821.

41 J. Zhou and I. Papautsky, *Microsyst. Nanoeng.*, 2020, **6**(1), 1–24.

42 S. Tamaki, H. Matsuzawa and M. Matsuhashi, *J. Bacteriol.*, 1980, **141**, 52–57.

43 B. Spratt, *Nature*, 1978, **274**, 713–715.

44 N. Iwai, K. Nagai and M. Wachi, *Biosci., Biotechnol., Biochem.*, 2002, **66**, 2658–2662.

45 P. Y. Huang, J. Feng, H. H. Hu and D. D. Joseph, *J. Fluid Mech.*, 1997, **343**, 73–94.

46 M. Li, M. van Zee, K. Goda and D. di Carlo, *Lab Chip*, 2018, **18**, 2575–2582.

47 F. Tian, W. Zhang, L. Cai, S. Li, G. Hu, Y. Cong, C. Liu, T. Li and J. Sun, *Lab Chip*, 2017, **17**, 3078–3085.

48 C. Liu, J. Guo, F. Tian, N. Yang, F. Yan, Y. Ding, J. Wei, G. Hu, G. Nie and J. Sun, *ACS Nano*, 2017, **11**, 6968–6976.

49 T. Rosén, A. Nordmark, C. K. Aidun, M. Do-Quang and F. Lundell, *Phys. Rev. Fluids*, 2016, **1**, 044201.

50 H. Huang and X. Y. Lu, *J. Fluid Mech.*, 2017, **822**, 664–688.

51 G. D'Avino, M. A. Hulsen, F. Greco and P. L. Maffettone, *J. Non-Newtonian Fluid Mech.*, 2019, **263**, 33–41.

52 P. L. Mage, A. T. Csordas, T. Brown, D. Klinger, M. Eisenstein, S. Mitragotri, C. Hawker and H. T. Soh, *Nat. Mater.*, 2019, **18**, 82–89.

53 J. Zhou and I. Papautsky, *Lab Chip*, 2013, **13**, 1121–1132.